Zeolite A imidazolate frameworks

HIDEKI HAYASHI[1]*, ADRIEN P. CÔTÉ[1], HIROYASU FURUKAWA[1], MICHAEL O'KEEFFE[2] AND OMAR M. YAGHI[1]*

[1]Department of Chemistry and Biochemistry, Center for Reticular Chemistry, University of California, Los Angeles, 607 Charles E. Young Drive East, Los Angeles, California 90095-1569, USA

[2]Department of Chemistry and Biochemistry, Arizona State University, Tempe, Arizona 85287-1604, USA

*e-mail: hhideki@chem.ucla.edu; yaghi@chem.ucla.edu

Published online: 27 May 2007; doi:10.1038/nmat1927

Faujasite (FAU) and zeolite A (LTA) are technologically important porous zeolites (aluminosilicates) because of their extensive use in petroleum cracking and water softening[1,2]. Introducing organic units and transition metals into the backbone of these types of zeolite allows us to expand their pore structures, enhance their functionality and access new applications[3,4]. The invention of metal–organic frameworks and zeolitic imidazolate frameworks (ZIFs) has provided materials based on simple zeolite structures where only one type of cage is present[5–9]. However, so far, no metal–organic analogues based on FAU or LTA topologies exist owing to the difficulty imposed by the presence of two types of large cage (super- and β-cages for FAU, α- and β-cages for LTA). Here, we have identified a strategy to produce an LTA imidazolate framework in which both the link geometry and link–link interactions play a decisive structure-directing role. We describe the synthesis and crystal structures of three porous ZIFs that are expanded analogues of zeolite A; their cage walls are functionalized, and their metal ions can be changed without changing the underlying LTA topology. Hydrogen, methane, carbon dioxide and argon gas adsorption isotherms are reported and the selectivity of this material for carbon dioxide over methane is demonstrated.

We[9] and others[10] have recently been systematically exploring metal–organic frameworks (MOFs) based on metal imidazolates that share many riches of zeolite chemistry, and because of their exceptional thermal and chemical stability[9], hold great promise as porous materials for a variety of applications. The frameworks of these compounds can be formulated as $T(Im)_2$ (Im = imidazolate and its derivatives, T = tetrahedrally bonded metal ion) and are similar to the $(Al)SiO_2$ frameworks of (alumino)silicate zeolites; in particular the T–Im–T angle of 145° is close to the Si–O–Si angle typically found in zeolites. Not surprisingly, we have found, for example, that for materials with both the RHO and SOD zeolite topologies, the same framework composition is obtained using benzimidazolate as a linker[9] (Fig. 1). In each of these structures there is only one type of cage. In our efforts to prepare a zeolitic imidazolate framework (ZIF) with zeolite A (LTA) topology, which has two types of cage (α and β), we found that replacing carbon atoms with nitrogen at key positions has a profound impact on whether or not the LTA structure is achieved (Fig. 1). Replacing carbon in position 4 of benzimidazolate gave ZIF-23 with a diamond topology. However, replacing the carbon atoms at position(s) 5 or 5 and 7 gave ZIFs based on LTA structures. As will be explained below, these positions are ideally suited for introducing link–link interactions and, together with the geometric control imparted by the nitrogen atoms in positions 1 and 3, direct the structure specifically to LTA (Fig. 1). This approach is a new way to exploit structure-directing agents, which also serve as linkers, in contrast to the addition of alkylammonium ions and some organic molecules that are well studied in the synthesis of aluminosilicate zeolites[11,12].

The new ZIFs with LTA topology were synthesized by a solvothermal reaction of $Zn(NO_3)_2{\cdot}4H_2O$ or $Co(NO_3)_2{\cdot}6H_2O$ and an excess amount of purine in *N,N*-dimethylformamide (DMF) at 65 °C or 85 °C, respectively, to give crystalline $Zn(Pur)_2{\cdot}(DMF)_{0.75}(H_2O)_{1.5}$ (ZIF-20, Pur = purinate) and its Co(II) analogue [ZIF-21, $Co(Pur)_2{\cdot}(DMF)(H_2O)$].

The structure of ZIF-20 was determined from single-crystal X-ray diffraction data. The framework of the LTA structure is illustrated in Fig. 2, which shows only the vertices (T atoms) and edges (links between the T atoms). It is simply made up of a tiling of cubes, truncated octahedra (β-cages) and truncated cuboctahedra (α-cages) in the ratio 3:1:1. In ZIF-20, the T atoms are Zn and the linkers are Pur bonding to Zn via the N atoms of the five-membered imidazolate ring (Fig. 3). In this structure the linkers are disordered, because the N and C atoms in the six-membered ring span a crystallographic mirror plane perpendicular to the ring and are therefore indistinguishable. A cubic unit cell of ZIF-20 with $a = 45.4725(2)$ Å contains 192 zinc ions within a unit cell volume of 94,025.7(7) Å^3. The density (T/V) of metal atoms per unit volume is 2.04 nm^{-3}, which is much less than that of zeolite A (12.9 nm^{-3}) (ref. 13). An identical structure where Co replaces Zn, ZIF-21, was also crystallized (see the Supplementary Information).

Figure 3 shows the separate cages in the structure of ZIF-20; note that, because of the way the Pur linkers are oriented, there are two types of α-cage, as shown in Fig. 3a,b. The α-cage consists of 48 Zn ions and 72 Pur (360 C, 216 H, 288 N). The large pore with a diameter of 14.5 Å (Fig. 3a) or 15.4 Å (Fig. 3b) is surrounded by 12 eight-membered rings, eight 12-membered rings and six 16-membered rings, in which Zn and C atoms in position 2 of Pur were counted as points on rings. The largest 16-membered ring has a pore aperture of 2.8 Å in diameter. The T···T distance (about 5.9 Å) in ZIF-20 is extended by replacing oxide ions with imidazolate linkers (the corresponding Si···Si distance in aluminosilicates is about 3.0 Å), which results in a larger maximum pore size for the α-cage compared with that in zeolite A (11.4 Å) (ref. 14). The β-cage [24 Zn and 36 Pur (180 C, 108 H, 144 N)] (Fig. 3c) and the cube [8 Zn and 12 Pur (60 C, 36 H, 48 N)] (Fig. 3d) have smaller cavities (5.3 and 4.5 Å, respectively)

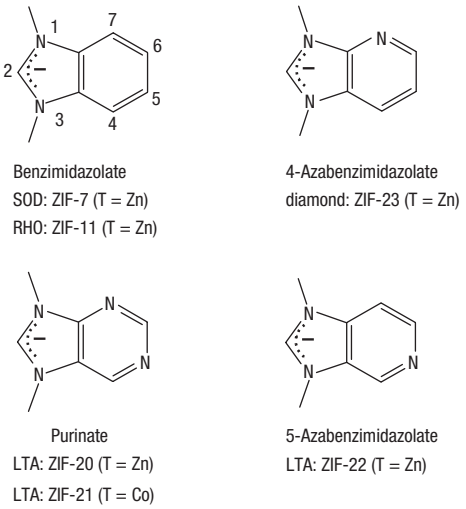

Figure 1 The positions of the nitrogen atoms in the imidazolate-type linkers are significant in determining which ZIF topology (SOD, RHO, diamond and LTA) is produced. The numbering of all linkers is the same as that indicated for benzimidazolate.

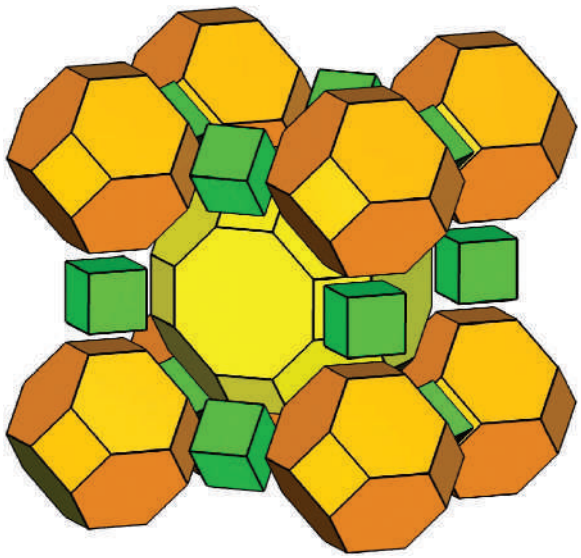

Figure 2 Cage constituents of the LTA topology. The structure is shown as an exploded tiling of cubes (green), truncated octahedra (orange) and truncated cuboctahedra (yellow).

and smaller pore apertures (2.0 Å and 1.5 Å, respectively). Thus, the α-cage can be accessed by some small molecules through the 16-membered window as described below.

To elucidate the reason for the formation of the LTA topology rather than the SOD and RHO (both obtained with benzimidazolate) (refs 9,13), we used either 4-azabenzimidazolate or 5-azabenzimidazolate as a linker (Fig. 1). The former gave a new structure (ZIF-23) with a diamond topology[15], but the latter led again to the LTA structure (ZIF-22) with essentially identical atomic coordinates as ZIF-20, both of which were identified by single-crystal X-ray crystallography (see the Supplementary Information).

It is clear that to produce the LTA structure, it is necessary to have a N atom at position 5 of the linker. Indeed, careful examination of all of these structures shows that a unique feature of the structure is (see, in particular, Fig. 3d) that pairs of atoms in six-membered rings at positions 5 and 6 (shown in red in the figure) are close to each other (3.39 and 3.52 Å). This seems to be caused by an electrostatic interaction and a dipole–dipole interaction between the CH—N···N—CH pair at positions 5 and 6 of the two linkers. However, in the case of 4-azabenzimidazolate, the distance between the two linkers at positions 4 and 7 is too great to form favourable interactions, as can be seen from Fig. 3d. Therefore, we believe that such interactions favour the formation of the cube, presumably at an early stage in crystallization of the LTA structure. The importance of the initial formation of the cube has also been proposed for zeolite A LTA synthesis[16].

Once the cube is formed, the LTA structure is the primary topological candidate that can propagate. As has been discussed elsewhere[17], there are only two ways of linking cubes through one type of edge and these lead to the LTA and ACO topologies[13], so we expect these to be the default topologies[5]. The LTA structure is already tailored to 145° T–X–T links (in our case X = Im), but in the maximum symmetry form of ACO that angle must be 180°. The angle in an ACO-derived structure can be decreased by lowering the symmetry, but, and this is a key point, to make an imidazolate ACO the T–Im bonds would have to be distorted significantly away from the plane of the linking molecule, in our case the five-membered $C_3H_1N_2$ imidazolate ring[17]. In fact, for all of the imidazolates we have examined, the T–Im bonds are coplanar with the imidazolate ring; for example, in ZIF-20 the Zn–N–N–Zn dihedral angles range from 0—0.15° and the cubes can be linked with a 145° angle and a planar linker (Fig. 3e).

The permanent porosity of guest-free (activated) ZIF-20 was confirmed by gas adsorption measurements. As-synthesized ZIF-20 consists of approximately 21 wt% DMF and H_2O molecules, as quantified from thermogravimetric analysis (TGA) corroborated by elemental microanalysis (see Supplementary Information, Fig. S9). The activated sample was prepared by exchanging the solvent in as-synthesized ZIF-20 with methanol, followed by evacuation at room temperature. The methanol-exchanged and activated compounds were characterized by TGA and powder X-ray diffraction measurements to assure full activation was achieved (see Supplementary Information, Figs S9 and S5, respectively).

The type-I isotherm (International Union of Pure and Applied Chemistry classification) observed for Ar adsorption at 87 K (Fig. 4a) indicates the microporosity of activated ZIF-20. The small H_4 hysteresis at relative pressure $P/P_0 > 0.4$ (where P_0 is the saturated vapour pressure of the adsorptive at the temperature of measurement and P is the equilibrium pressure) can be attributed to intercrystalline voids in the sample (see the Supplementary Information)[18]. The maximum pore aperture (2.8 Å) of ZIF-20, as measured from its crystal structure, is smaller than the kinetic diameter of Ar (3.40 Å). However, the space inside the structure becomes accessible through a dynamic aperture-widening process wherein the Pur swing out of the way to allow gas molecules to pass. The apparent surface area and pore volume were calculated to be 800 $m^2 g^{-1}$ and 0.27 $cm^3 g^{-1}$ by applying the Langmuir and Dubinin–Radushkevitch equation, respectively.

Adsorption isotherms for H_2 were collected at 77 and 87 K as shown in Fig. 4b. It should be noted that the repeatability of the H_2 adsorption behaviour was confirmed by reproducing the same isotherm four times at 77 K (see Supplementary Information, Fig. S15). The uptake at ~800 torr at 77 K is 1.1 wt%, which is slightly lower than those for ZIF-8 (1.3 wt%) and ZIF-11 (1.4 wt%) (ref. 9). The initial uptake of ZIF-20, however, is much higher than that of ZIF-8 and is

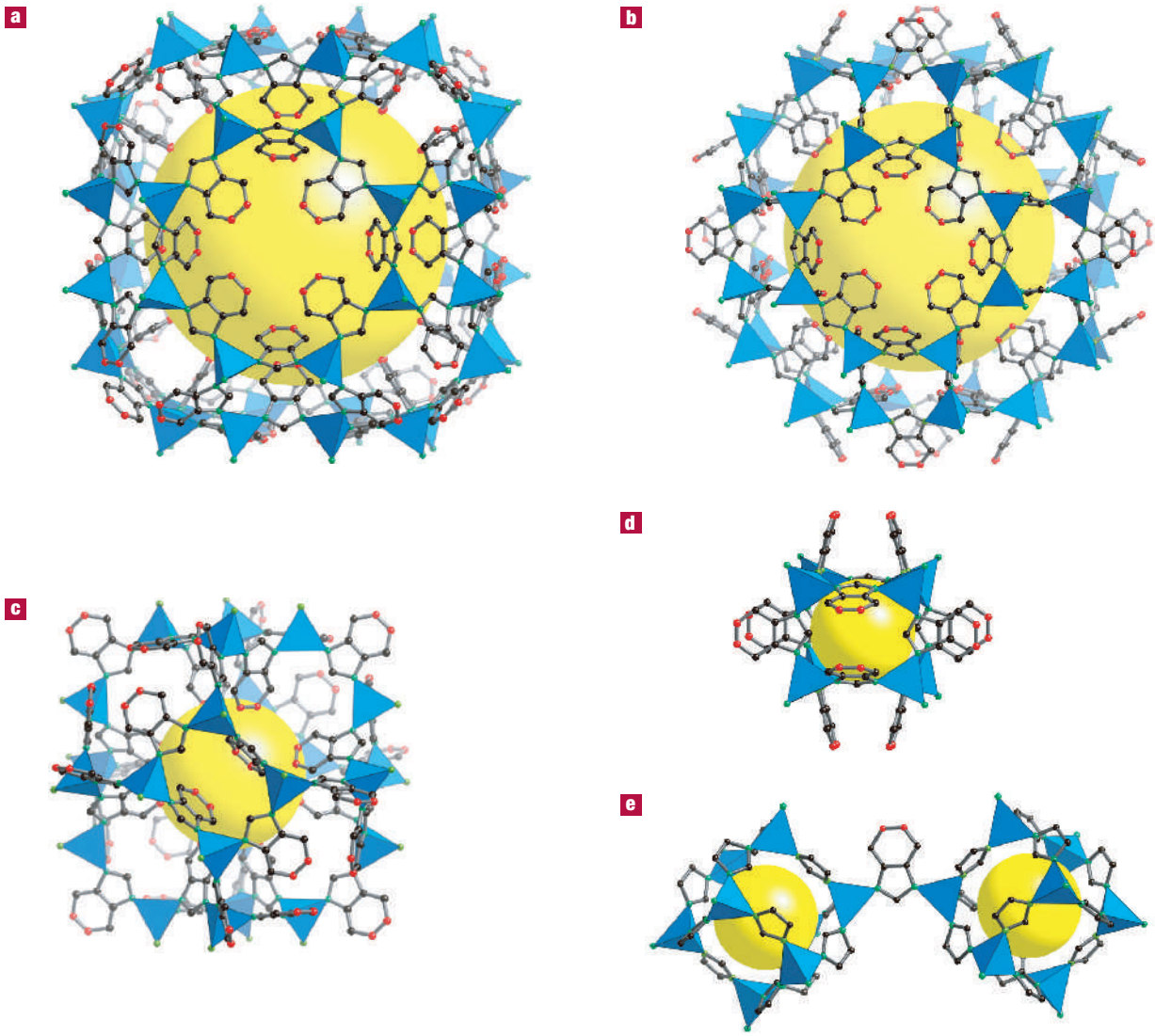

Figure 3 X-ray single-crystal structure of ZIF-20 with the same LTA topology as zeolite A. a–d, Here the oxygen and silicon atoms in zeolite A are replaced by purinates and tetrahedral zinc atoms, respectively, to give two expanded α-cages (**a**,**b**), a β-cage (**c**) and a cube (**d**). **e**, The formation of links between cubes is important in the reticulation of the structure. Note the pairs of interacting C/N atoms highlighted in red. ZnN_4 tetrahedra: blue; carbon and nitrogen at Pur position 7: black; nitrogen at Pur positions 1 and 3: green.

comparable to that of ZIF-11. This suggests that a relatively strong interaction between the ZIF-20 framework and H_2 exists. The presence of a strong interaction was also expected by the analysis of the isosteric heat of adsorption, (Q_{st}), which is calculated using parameters obtained by fitting the isotherms at 77 K and 87 K to a virial-type expression[19,20] (see Supplementary Information for details). The initial Q_{st} value is estimated to be 8.5 kJ mol^{-1}, which is relatively high compared with the other porous materials[20], such as some porous MOFs with small pores[21]. In addition, a theoretical study suggests that nitrogen atoms on aromatic rings in a framework can enhance the adsorption energy of H_2 (ref. 22). In our case, both effects are available to bind H_2 strongly.

The adsorption of CO_2 and CH_4 gas by ZIF-20 were also examined at 273 K. As shown in Fig. 4c, the CO_2 uptake at 760 torr is five times higher than that of CH_4, suggesting a stronger interaction between the framework and the CO_2 molecules. This behaviour led us to examine the separation of CO_2 from CH_4, which is an essential industrial process for natural-gas purification/combustion and landfill gas separation[23]. A preliminary breakthrough experiment (see the Methods section and Supplementary Information, Fig. S16) using a CO_2/CH_4 (about 50:50 v/v) gas mixture was carried out in a column packed with activated ZIF-20. Indeed, the breakthrough curves clearly show that ZIF-20 can separate CO_2 from CH_4 (Fig. 4d). This gas-separation behaviour is probably the result of uncoordinated nitrogen atoms inducing a polar pore wall, thus favourable CO_2 binding sites, and/or the appropriate pore size that prefers CO_2 rather than CH_4. Further work is in progress to fully understand the effect of the functionality for gas storage and separation properties of ZIFs and will be reported in future.

ZIFs are a new class of porous materials that potentially have the advantages of both inorganic zeolites (for example, high stability) and of MOFs (for example, high porosity and organic functionality), which could be applied to highly efficient

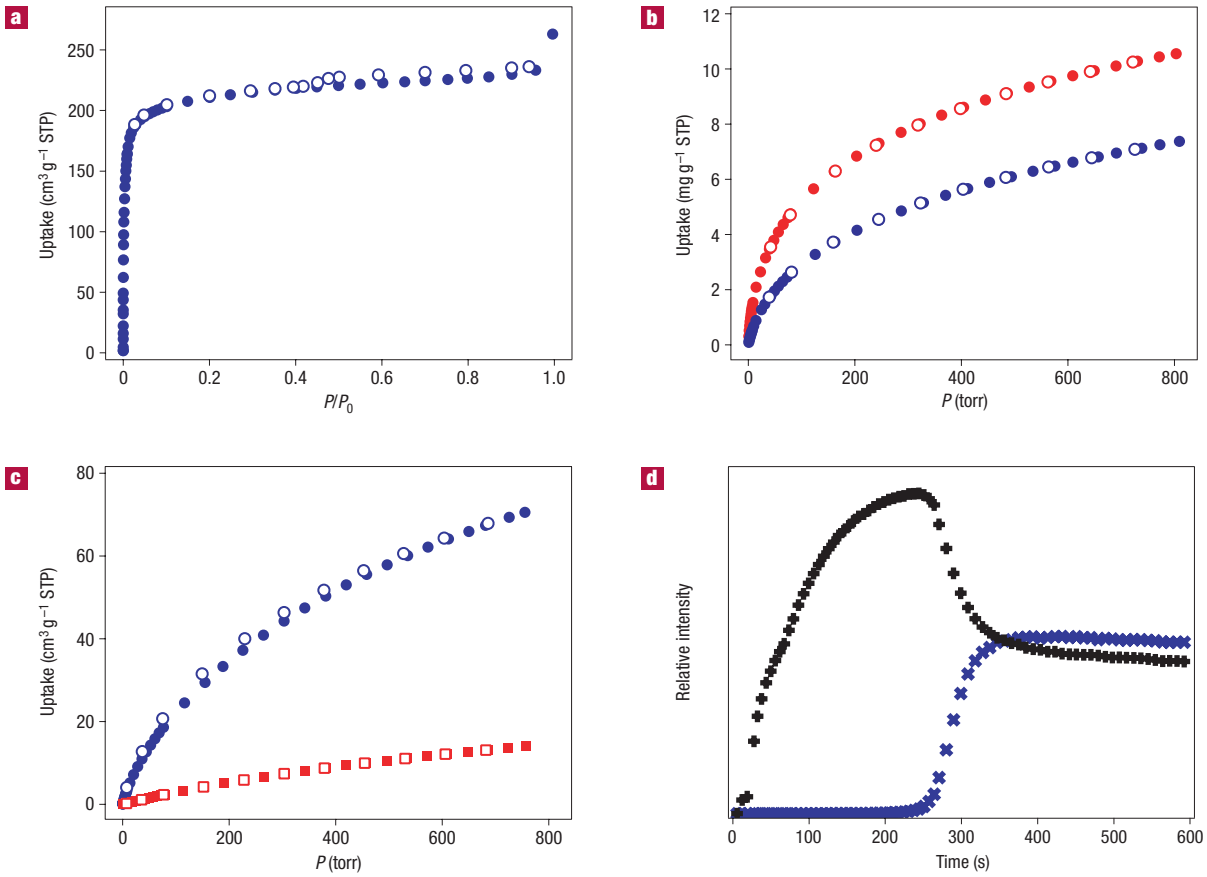

Figure 4 Gas adsorption isotherms of ZIF-20. a–c, For Ar at 87 K (**a**), H_2 at 77 K (red) and 87 K (blue) (**b**) and CO_2 (blue) and CH_4 (red) at 273 K (**c**). The filled and open circles represent adsorption and desorption, respectively. STP means standard temperature and pressure. **d**, Breakthrough curves of CO_2 (blue) and CH_4 (black) for ZIF-20 using a CO_2/CH_4 gas mixture. ZIF-20 has not only a permanent porosity, but also shows gas-separation ability. The relative intensities of each gas passing through the ZIF-20-packed column were obtained using a mass spectrometer to detect ion peaks at $m/z = 44$ (CO_2) and 16 (CH_4).

catalysis and separation processes. From a synthetic perspective, ZIF topologies can be directed by the molecular structure of the organic linker and rationalized by examining the resulting linker–linker interactions in the ZIFs. The potential difficulty in predicting ZIF structures, such as is always encountered in zeolite chemistry, can be overcome by further detailing the linker requirements for forming the basic secondary building units (cubes in the case of LTA) in the structure. The accumulation of such information should allow the development of strategies based on the principles of reticular chemistry[24] to create new zeolite structures with organic and transition-metal units.

METHODS

SYNTHESIS OF COMPOUNDS

ZIF-20: $Zn(Pur)_2{\cdot}(DMF)_{0.75}(H_2O)_{1.5}$. A solid mixture of zinc nitrate tetrahydrate $Zn(NO_3)_2{\cdot}4H_2O$ (65 mg, 0. 25 mmol, EM Science) and purine (150 mg, 1.25 mmol, Fluka or Sigma) was dissolved in 5 ml DMF (Fisher) in a 20 ml vial to obtain a slightly turbid solution. The vial was tightly capped and heated at 65 °C in an isothermal oven for 3 days to yield pale yellow octahedral crystals along with a small amount of powder. After unassisted cooling of the vial to room temperature, the powder product was removed by decanting with mother liquor and washed three times with DMF (5 ml). The crystals were dried in air for 30 min (yield: 48 mg, 50% based on $Zn(NO_3)_2{\cdot}4H_2O$). *Elemental analysis*: Calculated for $Zn(Pur)_2{\cdot}(DMF)_{0.75}(H_2O)_{1.5}$: C, 38.17; H, 3.73; N, 31.80. Found: C, 37.93; H, 3.52; N, 31.85%. Fourier-transform infrared (KBr, 4,000−400 cm^{-1}): 3,433(br), 3,098(w), 3,065(w), 3,036(w), 2,930(w), 2,856(w), 1,670(s), 1,589(s), 1,568(m), 1,477(s), 1,398(s), 1,310(s), 1,221(s), 1,192(m), 1,094(m), 1,020(w), 924(m), 804(m), 791(m), 683(w), 644(m), 621(w), 575(w), 498(w), 403(w).

ZIF-21: $Co(Pur)_2{\cdot}(DMF)(H_2O)$. A solid mixture of cobalt(II) nitrate hexahydrate $Co(NO_3)_2{\cdot}6H_2O$ (146 mg, 0.502 mmol, Aldrich) and purine (300 mg, 2.50 mmol) was dissolved in DMF (5 ml) in a 20 ml vial. To the solution, 2.0 M dimethylamine solution in methanol (1.25 ml, 2.50 mmol, Aldrich) was added. The vial was tightly capped and heated at 85 °C in an isothermal oven for 24 h to yield purple octrahedral crystals. After unassisted cooling of the vial to room temperature, the mother liquor was decanted and the crystals were rinsed three times with DMF (5 ml) and dried in air for 1 h (yield: 92 mg, 47% based on $Co(NO_3)_2{\cdot}6H_2O$). *Elemental analysis*: Calculated for $Co(Pur)_2{\cdot}(DMF)(H_2O)$: C, 40.22; H, 3.89; N, 32.47. Found: C, 40.36; H, 3.93; N, 32.16%. Fourier-transform infrared (KBr, 4,000−400 cm^{-1}): 3,418(br), 3,086(w), 2,924(w), 2,855(w), 1,665(s), 1,589(s), 1,560(m), 1,468(s), 1,443(w), 1,396(s), 1,308(s), 1,234(w), 1,207(s), 1,188(s), 1,109(m), 916(m), 804(m), 791(w), 677(w), 648(m), 623(w), 573(w), 500(w).

ZIF-22: $Zn(5\text{-Azabenzimidazolato})_2{\cdot}(DMF)_{0.75}(H_2O)_2$. A solid mixture of zinc nitrate tetrahydrate $Zn(NO_3)_2{\cdot}4H_2O$ (52 mg, 0.20 mmol) and 5-azabenzimidazole (238 mg, 2.00 mmol, Aldrich) was dissolved in 2 ml DMF in a 4 ml vial to obtain a white precipitate. The vial was tightly capped and heated at 150 °C in an isothermal oven for 3 days to yield pale yellow octahedral crystals along with a small amount of powder. After unassisted cooling of the vial to room temperature, the powder product was removed by decanting with mother liquor and rinsed three times with DMF (4 ml × 3). The crystals were

dried in air for 30 min (yield: 68 mg, 87% based on $Zn(NO_3)_2{\cdot}4H_2O$). *Elemental analysis*: Calculated for Zn(5-Azabenzimidazolato)$_2{\cdot}(DMF)_{0.75}(H_2O)_2$: C, 43.61; H, 4.43; N, 24.09. Found: C, 43.74; H, 4.33; N, 24.24%. Fourier-transform infrared (KBr, 4,000−400 cm^{-1}): 3,422(br), 3,067(br), 2,930(w), 2,858(w), 1,672(s), 1,601(s), 1,572(w), 1,468(s), 1,439(m), 1,408(w), 1,385(s), 1,342(w), 1,313(s), 1,285(m), 1,234(s), 1,205(w), 1,186(m), 1,173(w), 1,096(m), 1,063(w), 1,038(w), 1,016(m), 991(w). 918(s), 816(m), 793(m), 660(m), 644(m), 613(m), 565(w), 467(w), 420(w).

ZIF-23: Zn(4-Azabenzimidazolato)$_2{\cdot}(H_2O)_{0.25}$. A solid mixture of zinc nitrate tetrahydrate $Zn(NO_3)_2{\cdot}4H_2O$ (52 mg, 0.20 mmol) and 4-azabenzimidazole (119 mg, 1.00 mmol, Aldrich) was dissolved in 1 ml DMF in a 4 ml vial. The vial was tightly capped and heated at 100 °C in an isothermal oven for 1 day to yield pale yellow prism crystals. After unassisted cooling of the vial to room temperature, the crystals were rinsed three times with DMF (5 ml) and dried in air for 30 min (yield: 55 mg, 90% based on $Zn(NO_3)_2{\cdot}4H_2O$). The same product was obtained in reactions at different temperatures (65 and 150 °C), at which ZIF-20 and ZIF-22 were synthesized, respectively. Reaction with a different ligand/metal ratio (1:10, instead of 1:5) as used in the synthesis of ZIF-21 also gave the same compound. *Elemental analysis*: Calculated for Zn(4-Azabenzimidazolato)$_2{\cdot}(H_2O)_{0.25}$: C, 47.08; H, 2.80; N, 27.45. Found: C, 47.00; H, 2.82; N, 27.84%. Fourier-transform infrared (KBr, 4,000−400 cm^{-1}): 3,439(br), 3,080(m), 3,053(m), 2,937(w), 1,919(w), 1,879(w), 1,850(w), 1,665(m), 1,597(s), 1,574(w), 1,474(s), 1,406(s), 1,395(w), 1,313(m), 1,290(s), 1,263(w), 1,225(m), 1,186(m), 1,117(w), 1,042(w), 1,013(w), 959(w), 918(m), 802(m), 771(s), 667(m), 652(s), 594(w), 569(w), 503(m), 490(w).

MEASUREMENTS

Powder X-ray diffraction data were collected using a Bruker D8-Discover θ–2θ diffractometer in reflectance Bragg–Brentano geometry at 40 kV, 40 mA (1,600 W) for Cu Kα radiation ($\lambda = 1.5406$ Å). TGA was carried out using a TA Q500 thermal analysis system. Fourier-transform infrared spectra of samples prepared as KBr pellets were measured using a Nicolet FT-IR Impact 400 system.

SINGLE-CRYSTAL X-RAY DIFFRACTION STUDIES

Data were collected using a Bruker SMART APEXII three-circle diffractometer equipped with a CCD (charge-coupled device) area detector operated at 1,200 W power (40 kV, 30 mA) to generate Cu Kα radiation ($\lambda = 1.5418$ Å). All crystals were mounted on nylon CryoLoops (Hampton Research) with Paratone-N oil (Hampton Research). For all cases, frame widths of 0.5° were judged to be appropriate and full hemispheres of data were collected using the Bruker APEX2 software suite to carry out overlapping ϕ and ω scans at three different detector (2θ) settings ($2\theta = 28, 60, 100$°). Data were integrated with SAINT software using a narrow-frame algorithm and subsequently corrected for absorption. All structures were solved by direct methods and refined using the SHELXTL'97 software suite. Crystal data for ZIF-20: $C_{20}H_{12}N_{16}O_{8.88}Zn_2$, $M_r = 749.20$, cubic, space group $Fm\bar{3}m$, $a = 45.4725(2)$ Å, $V = 94{,}025.7(7)$ Å^3, $Z = 96$, $d_{calc} = 1.270$ g cm^{-3}, $T = 153(2)$ K, crystal size $= 0.20 \times 0.20 \times 0.15$ mm^3, $\lambda = 1.54178$ Å. Refinement of 184 parameters on 2,446 independent reflections out of 34,673 measured reflections ($R_{int} = 0.0466$) led to $R1 = 0.0871$, $wR2 = 0.3160$ ($I > 2\sigma(I)$) and goodness-of-fit = 1.467 with the largest peak and hole of 1.717 and −0.805 e$^-$ Å^{-3}. Further details and the crystal data for ZIF-21, ZIF-22 and ZIF-23 are provided as Supplementary Information. Coordinates for these structures are freely available for download in .cif format from the Cambridge Crystallographic Data Centre (http://www.ccdc.cam.ac.uk).

GAS ADSORPTION MEASUREMENTS

The sample for the gas adsorption measurement was prepared as follows. The as-synthesized sample of ZIF-20 was immersed in anhydrous methanol in a glove box for 3 days; during the exchange the methanol was refreshed six times. The resulting methanol-exchanged sample of ZIF-20 in methanol was transferred to a quartz cell in a glove box and the solvent was roughly decanted using a pipette. The wet sample then was evacuated at ambient temperature for 12 h to yield an activated sample (about 200 mg) for gas adsorption measurements. The sample cell with a filler rod was attached to a valve in the glove box, which was kept closed until the start of the measurement, and was then attached to the instrument without exposing the sample to air.

Low-pressure gas adsorption experiments (up to 1 atm) were carried out on a Quantachrome AUTOSORB-1 automatic volumetric instrument. Ultrahigh-purity-grade gases were used in all adsorption measurements. The Ar (87 K), H_2 (77 and 87 K), CO_2 (273 K) and CH_4 (273 K) isotherms were measured using a liquid argon bath (87 K), a liquid nitrogen bath (77 K) and an ice bath (273 K), respectively.

An apparent surface area of 800 m^2 g^{-1} (Langmuir, the linearity of fitting, 0.999967) was obtained by using the data points on the adsorption branch of the Ar isotherm in the range $P/P_0 = 0.02$–0.10. A micropore volume of 0.27 cm^3 g^{-1} was obtained by applying the Dubinin–Radushkevitch equation (the linearity of fitting, 0.999781) in the range $P/P_0 = 0.02$–0.10. Surface adsorption due to the quartz cell and filler rod was below 0.4% of the observed uptake with the sample. The N_2 adsorption isotherm was also measured at 77 K (see Supplementary Information, Fig. S12), although the extremely slow diffusion through the tight pore apertures of ZIF-20 prevented us from recording a complete isotherm starting in the low-pressure region. From the N_2 isotherm, almost the same Langmuir surface area (790 m^2 g^{-1}, the linearity of fitting, 0.999986) and micropore volume (0.28 cm^3 g^{-1}, the linearity of fitting, 0.999415) were obtained.

GAS-SEPARATION EXPERIMENT

The gas-separation property of ZIF-20 was examined by a breakthrough experiment using a CO_2/CH_4 gas mixture (about 50:50 v/v). An activated sample (1.3 g) of ZIF-20 was packed into a stainless-steel column (0.46 innerdiameter × 17 cm) in a glove box. The column was then attached to gas-separation apparatus built as shown in Supplementary Information, Fig. S16 Helium gas was initially purged into the sample column. The column was cooled to 273 K using an ice bath. The gas mixture (20 psi) was dosed into the column at a flow rate of 20 ml min^{-1}. The relative amounts of the gases passing through the column were monitored on a Hiden Analytical HPR20 benchtop gas analysis system detecting ion peaks at m/z 44 (CO_2) and 16 (CH_4). The gentle rising slope of the CH_4 profile is due to the initial displacement of purged He gas.

Received 16 January 2007; accepted 19 April 2007; published 27 May 2007.

References

1. Van Bekkum, H., Flanigen, E. M., Jacobs, P. A. & Jansen, J. C. (eds) *Introduction to Zeolite Science and Practice* (Elsevier, Amsterdam, 2001).
2. Breck, D. W. *Zeolite Molecular Sieves* (Wiley, New York, 1974).
3. Wight, A. P. & Davis, M. E. Design and preparation of organic-inorganic hybrid catalysts. *Chem. Rev.* **102**, 3589–3614 (2002).
4. Yamamoto, K., Sakata, Y., Nohara, Y., Takahashi, Y. & Tatsumi, T. Organic-inorganic hybrid zeolites containing organic frameworks. *Science* **300**, 470–472 (2003).
5. Yaghi, O. M. *et al.* Reticular synthesis and the design of new materials. *Nature* **423**, 705–714 (2003).
6. Kitagawa, S., Kitaura, R. & Noro, S. Functional porous coordination polymers. *Angew. Chem. Int. Edn* **43**, 2334–2375 (2004).
7. Brant, J. A., Liu, Y., Sava, D. F., Beauchamp, D. & Eddaoudi, M. Single-metal-ion-based molecular building blocks (MBBs) approach to the design and synthesis of metal-organic assemblies. *J. Mol. Struct.* **796**, 160–164 (2006).
8. Zhang, J.-P. & Chen, X.-M. Crystal engineering of binary metal imidazolate and triazolate frameworks. *Chem. Commun.* 1689–1699 (2006).
9. Park, K. S. *et al.* Exceptional chemical and thermal stability of zeolitic imidazolate frameworks. *Proc. Natl Acad. Sci. USA* **103**, 10186–10191 (2006).
10. Huang, X.-C., Lin, Y.-Y., Zhang, J.-P. & Chen, X.-M. Ligand-directed strategy for zeolite-type metal-organic frameworks: Zinc(II) imidazolates with unusual zeolitic topologies. *Angew. Chem. Int. Edn* **45**, 1557–1559 (2006).
11. Lobo, R. F., Zones, S. I. & Davis, M. E. Structure-direction in zeolite synthesis. *J. Inclusion Phenom. Mol. Recognit. Chem.* **21**, 47–78 (1995).
12. Corma, A., Rey, F., Rius, J., Sabater, M. J. & Valencia, S. Supramolecular self-assembled molecules as organic directing agent for synthesis of zeolites. *Nature* **431**, 287–290 (2004).
13. Baerlocher, C., Meier, W. M. & Olson, D. H. *Atlas of Zeolite Framework Types* 5th edn (Elsevier, Amsterdam, 2001).
14. Breck, D. W., Eversole, W. G., Milton, R. M., Reed, T. B. & Thomas, T. L. Crystalline zeolites. I. The properties of a new synthetic zeolite, type A. *J. Am. Chem. Soc.* **78**, 5963–5971 (1956).
15. Rettig, S. J., Sánchez, V., Storr, A., Thompson, R. C. & Trotter, J. Polybis(4-azabenzimidazolato)-iron(II) and -cobalt(II). 3-D single diamond-like framework materials which exhibit spin canting and ferromagnetic ordering at low temperatures. *J. Chem. Soc., Dalton Trans.* 3931–3937 (2000).
16. Sugiyama, S. *et al.* AFM observation of double 4-rings on zeolite LTA crystals surface. *Micropor. Mesopor. Mater.* **28**, 1–7 (1999).
17. O'Keeffe, M. & Yaghi, O. M. Germanate zeolites: contrasting the behavior of germanate and silicate structures built from cubic T_8O_{20} units (T = Ge or Si). *Chem. Eur. J.* **5**, 2796–2801 (1999).
18. Vishnyakov, A., Ravikovitch, P. I., Neimark, A. V., Bülow, M. & Wang, Q. M. Nanopore structure and sorption properties of Cu-BTC metal-organic framework. *Nano Lett.* **3**, 713–718 (2003).
19. Czepirski, L. & Jagiełło, J. Virial-type thermal equation of gas-solid adsorption. *Chem. Eng. Sci.* **44**, 797–801 (1989).
20. Rowsell, J. L. C. & Yaghi, O. M. Effects of functionalization, catenation, and variation of the metal oxide and organic linking units on the low-pressure hydrogen adsorption properties of metal-organic frameworks. *J. Am. Chem. Soc.* **128**, 1304–1315 (2006).

21. Dincă, M., Yu, A. F. & Long, J. R. Microporous metal-organic frameworks incorporating 1,4-benzeneditetrazolate: syntheses, structures, and hydrogen storage properties. *J. Am. Chem. Soc.* **128**, 8904–8913 (2006).
22. Samanta, A., Furuta, T. & Li, J. Theoretical assessment of the elastic constants and hydrogen storage capacity of some metal-organic framework materials. *J. Chem. Phys.* **125**, 084714 (2006).
23. Sircar, S. Basic research needs for design of adsorptive gas separation processes. *Ind. Eng. Chem. Res.* **45**, 5435–5448 (2006).
24. Ockwig, N. W., Delgado-Friedrichs, O., O'Keeffe, M. & Yaghi, O. M. Reticular chemistry: Occurrence and taxonomy of nets and grammar for the design of frameworks. *Acc. Chem. Res.* **38**, 176–182 (2005).

Acknowledgements

This work was supported by BASF Ludwigshafen, Germany, US Department of Energy (DEFG0206ER15813) and Japan Society for Promotion of Science (Postdoctoral Fellowship, H.H.).
Correspondence and requests for materials should be addressed to H.H. or O.M.Y.
Supplementary Information accompanies this paper on www.nature.com/naturematerials.

Competing financial interests

The authors declare no competing financial interests.